Jpn J Ophthalmol (2014) 58:131–138
DOI 10.1007/s10384-013-0291-3

THE OFFICIAL INTERNATIONAL JOURNAL OF THE JAPANESE OPHTHALMOLOGICAL SOCIETY

CLINICAL INVESTIGATION

Characteristics of corneal topographic and pachymetric patterns in patients with pellucid marginal corneal degeneration

Mutsumi Fuchihata · Naoyuki Maeda · Ryotaro Toda · Shizuka Koh · Takashi Fujikado · Kohji Nishida

Received: 22 February 2013 / Accepted: 20 September 2013 / Published online: 3 December 2013

Abstract
Purpose To determine the characteristics of the shape of the cornea in patients with pellucid marginal corneal degeneration (PMD) and to compare these characteristics to those of eyes with keratoconus and eyes of normal subjects.
Methods This was a retrospective, cross-sectional case-series in which 49 eyes of 33 patients with PMD, 51 eyes of 51 patients with keratoconus and 53 eyes of 53 subjects with normal corneas (controls) were examined and compared. For all eyes, we obtained the topographic patterns of the axial power maps, anterior and posterior elevation maps and pachymetric maps using a rotating Scheimpflug camera. The eyes were classified into the respective patterns by visual inspection of these maps.
Results In eyes with PMD, the most common axial power map pattern was the crab claw pattern (78 %) followed by the inferior steepening pattern (18 %). In eyes with keratoconus, the most common pattern was the inferior steepening pattern (67 %). The most common pattern in the elevation maps for both surfaces was the asymmetric island in eyes with PMD and keratoconus. Although the decentered pattern, including the decentered oval (27 %) and decentered round (20 %) pattern, on pachymetric map was specific to eyes with PMD, the incidence of these patterns was relatively low.
Conclusions The similarity in the topographic and pachymetric patterns in eyes with PMD and keratoconus suggests that they may be a continuity of the same disorder with different phenotypes.

Keywords Corneal topography · Pellucid marginal corneal degeneration · Keratoconus · Topographic pattern · Scheimpflug camera

M. Fuchihata · N. Maeda (✉) · S. Koh · K. Nishida
Department of Ophthalmology, Osaka University Graduate School of Medicine, Room E7, 2-2 Yamadaoka, Suita, Osaka 565-0871, Japan
e-mail: nmaeda@ophthal.med.osaka-u.ac.jp

R. Toda
Department of Ophthalmology and Visual Science, Hiroshima University Graduate School of Biomedical & Health Sciences, Hiroshima, Japan

T. Fujikado
Department of Applied Visual Science, Osaka University Graduate School of Medicine, Osaka, Japan

Introduction

Pellucid marginal corneal degeneration (PMD) is a non-inflammatory, corneal thinning disorder in which the thinning occurs mainly at the inferior peripheral cornea [1]. Although PMD has been considered to be a variant of keratoconus [1–3], there are clinical differences between these two entities, such as age predilection [4, 5], effects of contact lenses [6, 7], surgical treatment [4, 8, 9] and topographic characteristics [1, 10, 11].

Careful preoperative screening is necessary to identify individuals with PMD to prevent them from undergoing LASIK (laser in-situ keratomileusis) because this procedure can lead to keratectasia [12, 13]. In addition, it is important to differentiate PMD from keratoconus to avoid an incorrect diagnosis that could lead to inappropriate treatment [14].

Detailed examinations of the anterior and posterior elevation maps and pachymetric maps of eyes with PMD have not been reported to date. Thus, the purpose of this study was to compare the topography of the anterior and

posterior corneal surfaces and the corneal thicknesses in eyes with PMD or keratoconus and control eyes.

Subjects and methods

Subjects

Patients with PMD who visited the Osaka University Hospital between January 2000 and December 2012 were enrolled in this study. In total, 49 eyes of 33 patients (30 men, 3 women; average age 37.8 ± 9.0 years) with PMD for whom reliable topographic measurements were available were studied. From the medical records of the hospital, we identified 51 age-matched keratoconic eyes of 51 patients (41 men, 10 women; average age 35.4 ± 11.4 years) and 53 normal eyes of 53 patients (39 men, 14 women; average age 39.8 ± 15.7 years), all with reliable topographic measurements, and used these eyes as reference.

The medical charts of patients with PMD or keratoconus and the controls were reviewed. A diagnosis of PMD was made when corneal thinning was found below the inferior pupil margin in eyes with severe against-the-rule astigmatism when tested in a dark room. The criteria for diagnosing keratoconus were the detection of stromal thinning in the central zone, Vogt's striae and/or Fleischer ring by slit-lamp biomicroscopy. Eyes with subclinical keratoconus or subclinical PMD were excluded. Controls were defined as those eyes with no signs of any ocular diseases expect for myopia or myopic astigmatism.

The research procedures conformed to the tenets of the Declaration of Helsinki, and the Institutional Review Board of Osaka University approved the procedures used in this study.

Measurement of corneal topography

A rotating single Scheimpflug-based corneal topographer (Pentacam HR; OCULUS Optikgeräte GmbH, Wetzlar, Germany) was used to measure the corneal topography. The diameter of the measured region was set to 12 mm [15]. The following settings were used to display the color-coded maps. The standard 1.5 diopter (D) Fix color bar from 27.0 to 72.0 D (1.5 D step) was used for the axial power maps. The American color-coded bar was used to display the anterior best-fit sphere (BFS) elevation maps, the posterior BFS elevation maps, and pachymetry (corneal thickness) maps. The anterior elevation map was fixed to an elevation scale of ±150 μm in 5-μm steps, and the posterior map was set to ±300 μm in 10-μm steps. The pachymetry map was fixed to 300–900 μm in 10-μm steps.

For the subjects who could not visit the hospital without wearing rigid gas permeable (RGP) contact lenses due to severe irregular astigmatism, the measurements were performed after removing the RGP contact lenses for at least 20 min.

Classification of axial power maps, elevation maps, and pachymetry maps

The axial power maps were classified into eight patterns: round, oval, symmetric bowtie, asymmetric bowtie, central steepening, lazy 8 figure, inferior steepening and crab claw

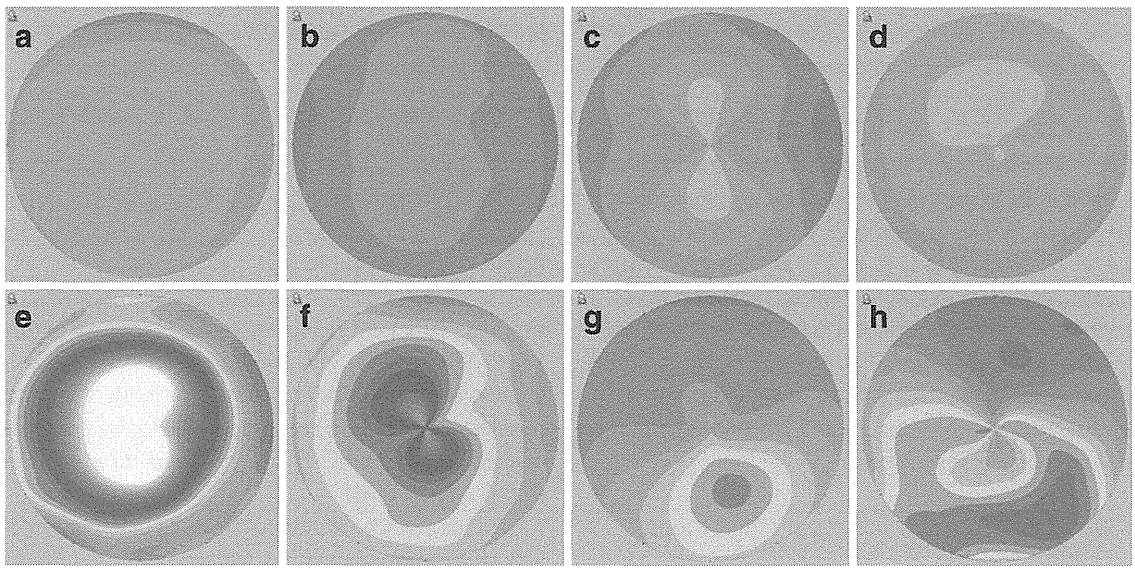

Fig. 1 Classification of the eight axial power map patterns. **a** Round pattern, **b** oval pattern, **c** symmetric bowtie pattern, **d** asymmetric bowtie pattern, **e** central steepening pattern, **f** lazy 8 figure pattern, **g** inferior steepening pattern, **h** crab claw pattern

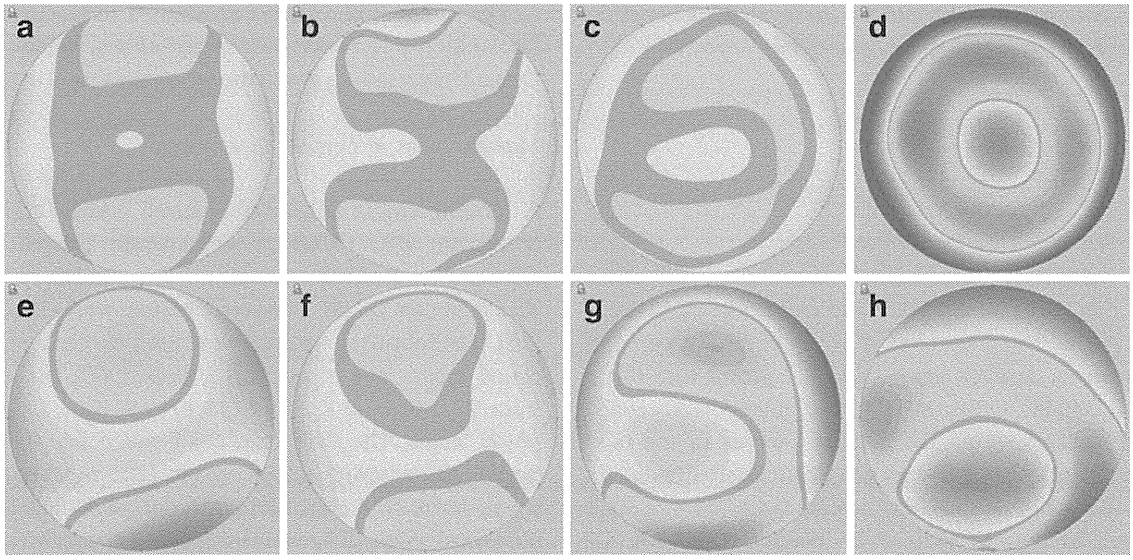

Fig. 2 Classification of eight elevation map patterns. **a** Central regular ridge pattern, **b** central irregular ridge pattern, **c** central incomplete ridge pattern, **d** central island pattern, **e** asymmetric regular ridge pattern, **f** asymmetric irregular ridge pattern, **g** asymmetric incomplete ridge pattern, **h** asymmetric island pattern

appearance (Fig. 1). The typical patterns for eyes with keratoconus and PMD were included in addition to those of the normal patterns described by Bogan [15–19].

The elevation maps were categorized into nine patterns: central regular ridge, central irregular ridge, central incomplete ridge, central island, asymmetric regular ridge, asymmetric irregular ridge, asymmetric incomplete ridge, asymmetric island and unclassified. This classification was modified from that of the normal pattern [20], and the possible patterns for eyes with keratoconus and PMD were added (Fig. 2).

The pachymetric maps were classified into six patterns: central round, central oval, paracentral round, paracentral oval, decentered round and decentered oval (Fig. 3). This classification was adapted from a previous study [21]. The term "central" was used when the location of the thinnest corneal point was located within the central 2-mm-diameter zone. When the point was beyond this 2-mm-diameter zone and within a 3-mm-diameter zone, the map was considered to be paracentral; if it fell outside the 3-mm-diameter zone, the map was classified as decentered.

These classification were performed by two ophthalmologists (MF, NM) who specialize in corneal topography. If the resulting classification differed between the two examiners, the maps were jointly examined once again and a consensus agreement was reached.

Relationship between steepest point and thinnest point

The corneal dioptric power at the steepest point (K_{max}) and its coordinates were recorded. Similarly, the corneal thickness at the thinnest point and its coordinates were determined. The relationship between the steepest point and thinnest point was compared among the three groups.

Statistical analyses

For the statistical analyses, the data were exported to Microsoft Excel (Microsoft, Redwood, WA) and analyzed using the Sigma plot software (ver. 12.0; SYSTAT Inc., Chicago, IL). One-way analysis of variance was used to compare results among the groups for the K_{max} and thinnest pachymetry. Linear regression analysis was used to determine the significance of the correlation between the value of the thinnest corneal point and the value of K_{max}. A P value of <0.05 was considered to be significant.

Results

Representative topographic patterns

In eyes with PMD (Fig. 4a), the axial power map had a crab claw pattern, and an asymmetric island was clearly visible on the elevation maps for both the anterior and posterior surfaces. The corneal thickness map had a decentered oval pattern. A corneal band thinning was present in the inferior area.

In eyes with keratoconus (Fig. 4b), the axial power map had an inferior steepening pattern, and the elevation maps for both surfaces had an asymmetric island pattern. The corneal thickness map had a paracentral round pattern.

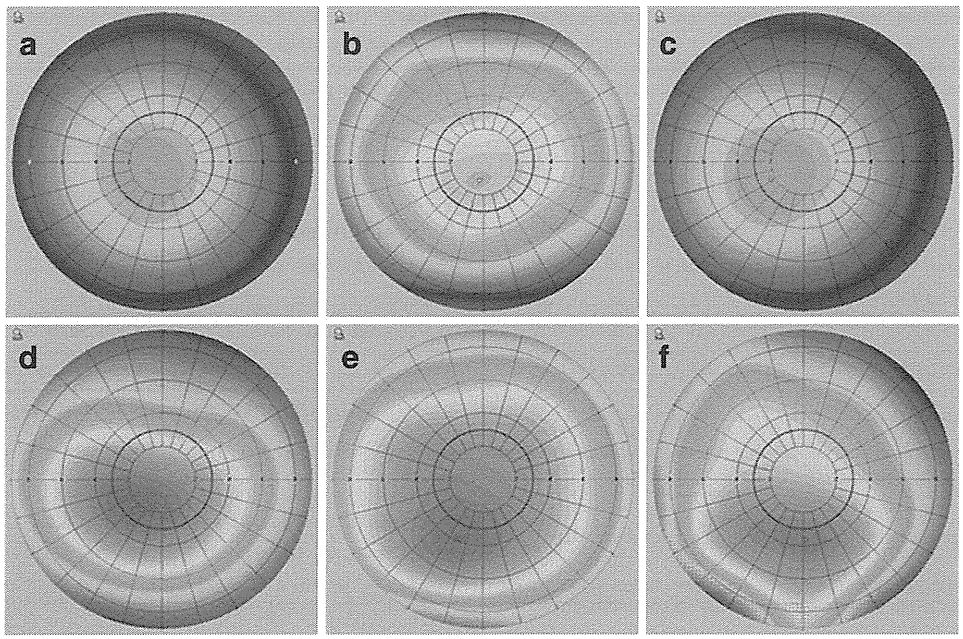

Fig. 3 Classification of six pachymetric map patterns. *Circles* indicate the 2-, 4-, 6- and 8-mm-diameter zones, respectively, *bold line* encircles the 3-mm-diameter zone, *open circles* designate the thinnest points. **a** Central round pattern, **b** central oval pattern, **c** paracentral round pattern, **d** paracentral oval pattern, **e** decentered round pattern, **f** decentered oval pattern

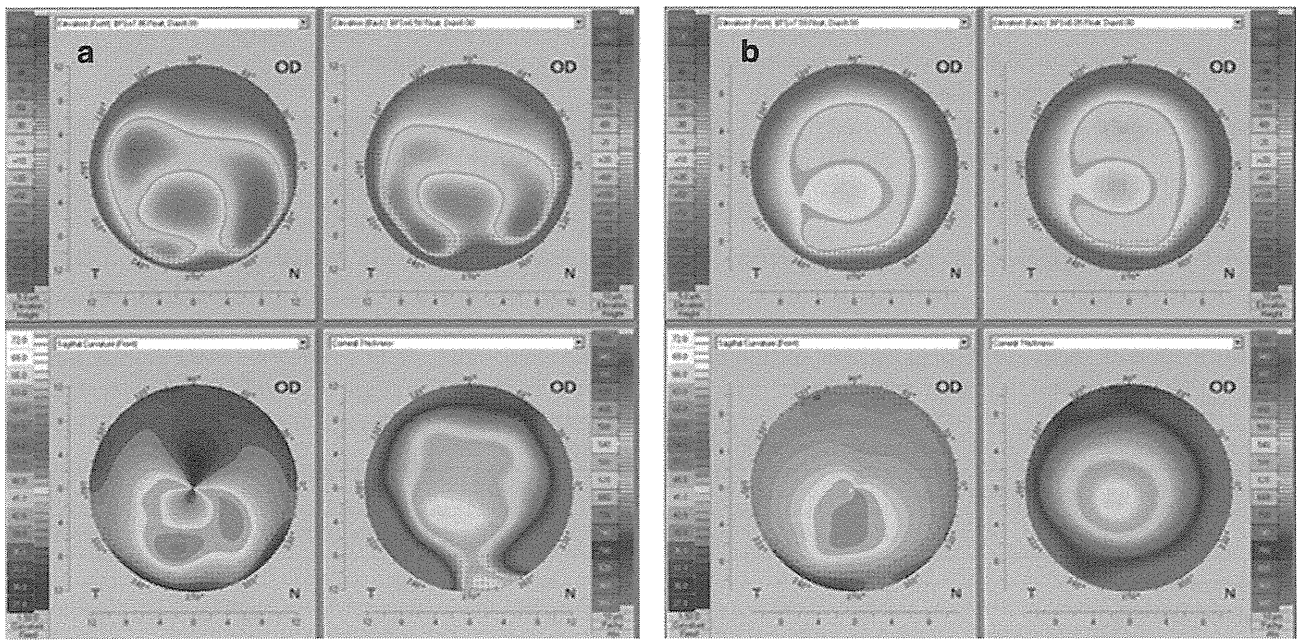

Fig. 4 Representative topographic patterns in pellucid marginal corneal degeneration (PMD) (**a**) and keratoconus (**b**). *Upper left image* Anterior elevation best-fit sphere, *upper right image* posterior elevation best-fit sphere, *lower left image* axial power map, *lower right* pachymetry map

Classification of topographic pattern in axial power maps

The topographic patterns in the axial maps of the three groups is listed in Table 1. The most common anterior topographic pattern in eyes with PMD was the crab claw pattern followed by the inferior steepening pattern. In comparison, the most frequent anterior topographic patterns in eyes with keratoconus was the inferior steepening pattern followed by the central steepening

Table 1 Classification of eyes in the axial power map according to topographic pattern

Topographic pattern in axial power map	PMD (%)	KC (%)	Control (%)
Round	0	0	58
Oval	0	0	11
Symmetric bowtie	0	0	26
Asymmetric bowtie	2	0	4
Central steepening	2	24	0
Lazy 8 figure	0	8	0
Inferior steepening	18	67	0
Crab claw	78	2	0
Total	100	100	100

Data are presented as the percentage of total eyes in the axial power map

PMD Pellucid marginal corneal degeneration, *KC* keratoconus

pattern. In controls, the round pattern was the most common.

Classification of topographic pattern in elevation maps

The patterns of the anterior and posterior elevation maps are listed in Table 2. Each group had similar trends for the anterior and posterior surfaces. The most common elevation pattern in eyes with PMD was the asymmetric island pattern. In eyes with keratoconus, the asymmetric island pattern was also the most common followed by the central island pattern. In controls, the central regular ridge pattern was the most frequent.

Classification of topographic patterns in pachymetric maps

The distribution of pachymetric map patterns for the three groups of eyes is shown in Table 3. The most common pachymetry pattern in eyes with PMD was the decentered oval pattern followed by decentered round pattern. In contrast, neither the decentered oval nor the decentered round patterns was seen in keratoconic and normal eyes. In eyes with keratoconus, the most frequent pachymetry pattern was a central round pattern followed by the paracentral round pattern. The most predominant pattern in control eyes was the central round pattern.

Table 3 Classification of eyes in the pachymetric map according to topographic pattern

Topographic pattern in the pachymetric map	PMD (%)	KC (%)	Control (%)
Central round	14	51	96
Central oval	8	18	0
Paracentral round	18	27	4
Paracentral oval	12	4	0
Decentered round	20	0	0
Decentered oval	27	0	0
Total	100	100	100

Data are presented as the percentage of total eyes in the elevation map

Corneal dioptric power at the steepest point and corneal thickness at the thinnest point

The value of K_{max} was 52.1 ± 5.70 D in eyes with PMD, 63.0 ± 10.9 D in eyes with keratoconus, and 44.6 ± 1.61 D in the control eyes. The power of K_{max} in the control eyes was significantly lower than that in keratoconic and PMD eyes ($P < 0.05$). The $X \times Y$ coordinates of K_{max} was $-0.10 \pm 1.51 \times -2.39 \pm 1.40$ mm in eyes with PMD, $0.12 \pm 0.43 \times -1.29 \pm 1.00$ mm in eyes with keratoconus and $0.02 \pm 0.82 \times -0.03 \pm 1.98$ mm in control eyes. The average Y coordinate was located in a

Table 2 Classification of eyes in the elevation map according to topographic pattern

Topographic pattern in the elevation map	PMD		KC		Control	
	Anterior (%)	Posterior (%)	Anterior (%)	Posterior (%)	Anterior (%)	Posterior (%)
Central regular ridge	2	2	4	2	70	57
Central irregular ridge	2	2	2	0	11	38
Central incomplete ridge	0	0	0	4	9	4
Central island	0	0	12	20	0	0
Asymmetric regular ridge	2	0	24	14	0	0
Asymmetric irregular ridge	6	0	6	0	0	0
Asymmetric incomplete ridge	8	2	16	20	0	0
Asymmetric island	80	92	37	41	0	0
Unclassified	0	2	0	0	9	2
Total	100	100	100	100	100	100

Data are presented as the percentage of total eyes in the elevation map

decentered zone in eyes with PMD, in a paracentral zone in eyes with keratoconus and in the central zone in controls. The average vertical (Y) coordinate in eyes with PMD was located significantly more inferiorly than that in eyes with keratoconus and control eyes ($P < 0.05$).

The corneal thickness at the thinnest point was 480.5 ± 45.8 μm in eyes with PMD, 421.3 ± 83.10 μm in eyes with keratoconus and 548.5 ± 27.74 μm in control eyes. The cornea in the control eyes was significantly thicker than that in eyes with keratoconus and PMD ($P < 0.05$). The mean location of the thinnest point in the XY coordinates was at $-0.28 \pm 0.52 \times -1.20 \pm 0.58$ mm in PMD eyes, $-0.40 \pm 0.31 \times -0.65 \pm 0.27$ mm in keratoconic eyes, and $-0.43 \pm 0.38 \times -0.44 \pm 0.24$ mm in control eyes. The vertical Y coordinate was located significantly more inferiorly in PMD eyes than in the other two groups of eyes ($P < 0.05$). In all groups, the average thinnest point was located at an infero-temporal point. The thinnest point was located closer to center than the K_{max} point in keratoconus and PMD eyes.

The value of the thinnest corneal point and the value of K_{max} was negatively correlated in eyes with PMD ($R = 0.390$, $P = 0.006$) and in eyes with keratoconus ($R = 0.613$, $P < 0.001$). In controls, there was no significant correlation between these values ($R = 0.022$, $P = 0.873$).

Relationship between thinnest points and positions of K_{max}

The positions of K_{max} and thinnest point are plotted in Fig. 5. In PMD, the thinnest point tended to be at the infero-temporal area, mainly at the paracentral zone. The distribution of K_{max} had two patterns; one was in the central zone and the other was in the inferior cornea at a more peripheral location than that of the thinnest point. In eyes with keratoconus, the thinnest point and K_{max} were closer to each other, with K_{max} located more inferiorly than that of thinnest point. In controls, the thinnest point was located mainly in the central zone, but it was also found in the infero-temporal area. However, K_{max} tended to be located in the superior or inferior area far from the center in cases of the bowtie pattern. The position of the thinnest point and that of the steepest point were separated.

Discussion

It is known that the typical topographic characteristic of the axial power map for eyes with PMD is the crab claw pattern. However, it has been reported that the crab claw pattern is not a diagnostic criterion of PMD because it is also seen in eyes with inferior keratoconus [15, 17]. In addition, there are to date no detailed reports on the patterns present in the elevation maps and the pachymetric maps for eyes with PMD.

Although a consensus exists that PMD is a variant of keratoconus, the borderline between both diseases is not well established, especially for mild cases. Our diagnosis in this study was based on slit-lamp findings. When corneal thinning was found below the inferior pupil margin in eyes with high against-the-rule astigmatism, we were diagnosed these eyes as having PMD. Our rationale was that the protrusion within the pupillary margins will create a steep apex, and the protrusion below the pupillary margins will create a flat curvature in the center and against-the-rule astigmatism. These are the typical findings for both diseases. Some of our cases might have been diagnosed as inferior keratoconus by other investigators. In addition, there may be intermediate cases between PMD and

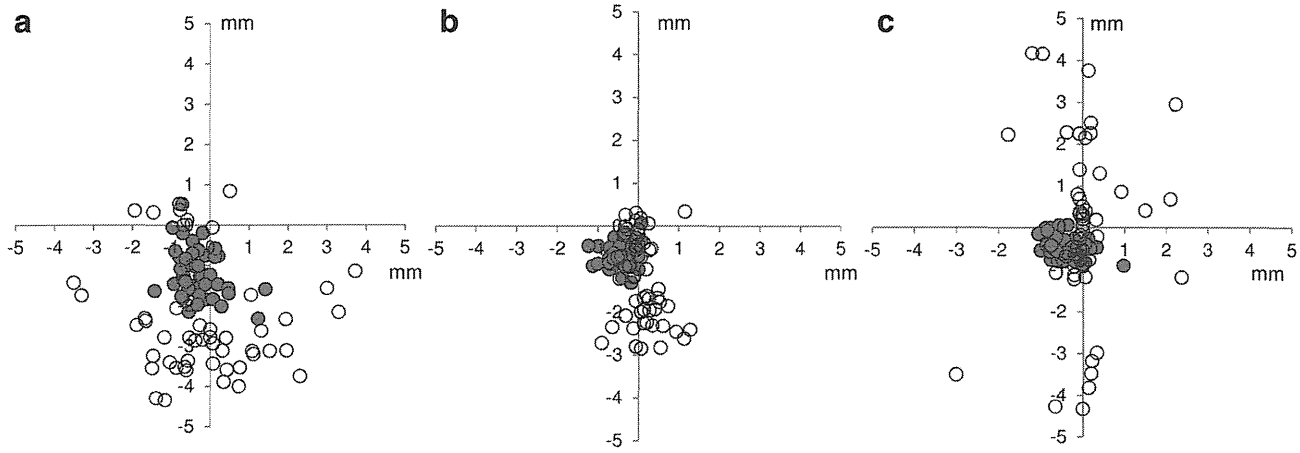

Fig. 5 Distribution of thinnest corneal point. **a** PMD, **b** keratoconus, **c** normal cornea. *Filled circle* pachymetry, *open circle* corneal dioptric power at the steepest point (K_{max})

keratoconus, and it is difficult to differentiate PMD from keratoconus, especially in an early stage, by topographic analysis. Therefore, it is important to be able to identify not only the specific patterns for keratoconus and PMD but also the common features of both diseases.

The borderline between PMD and keratoconus was set at the lower pupil margin for the location of corneal thinning in the slit-lamp examinations. Based on this definition, the crab claw pattern in the axial power map was specific to PMD and the localized steepening was specific to keratoconus. The central island pattern in the elevation maps of the anterior or posterior surfaces was specific to keratoconus, but the incidence was low. An asymmetric ridge pattern and asymmetric island pattern were common patterns in eyes with PMD and keratoconus. For the pachymetric maps, decentered round and decentered oval patterns were seen only in eyes with PMD. These findings from the elevation and pachymetric maps are in keeping with the peripheral thinning. Our results indicate that there are many overlaps in the topographic patterns between the eyes with PMD and keratoconus, respectively.

In our eyes with PMD, the average thinnest point was in the infero-temporal paracentral zone, while the K_{max} was present at two locations—one in the central zone and the other scattered in the inferior peripheral zone. In most of our eyes with PMD, we found that the peripheral cornea was not thinner than the central zone even if there was an obvious difference in the corneal thickness between the inferior peripheral area and the other peripheral areas.

In contrast, in eyes with keratoconus, the thinnest point was mainly at the inferior paracentral zone, and K_{max} was close to the thinnest point in these eyes. In contrast, in control eyes, the thinnest point was mainly located at the inferior central zone, and the K_{max} points were closer to the Y-axis in these eyes. The K_{max} points were distributed in the upper or inferior peripheral zone corresponding to the bowtie pattern due to the with-the-rule astigmatism. The relationships of the location of K_{max} and the thinnest corneal point might be useful factors to differentiate PMD from keratoconus.

There are some limitations to our study. Because of the rareness of this disease, the number of cases with PMD was small, and there might be some bias in the selection of patients because this was a retrospective, cross-sectional, case-series study. A prospective study of the characteristics of the corneal shapes will be necessary to definitively distinguish PMD from keratoconus. As many topographic programs for detecting keratoconus do not use PMD as their target [22], it might be a good idea to develop a program that detects both keratoconus and PMD for the screening of refractive surgery.

Belin et al. [15] proposed that all studies associated with PMD should analyze the full pachymetric map covering the central 12 mm of the cornea. We examined the corneal maps for the central 12-mm-diameter zone and found that most of the data outside the 9-mm-diameter zone were extrapolated not only in eyes with PMD but also in those with keratoconus—at least in this Japanese population. Therefore, even if reproducible topographic maps had been obtained in our study, only the topographic data within a 9-mm-diameter central area could be analyzed.

An accurate topographic analysis could not be performed for eyes with advanced PMD. The recently developed optical coherence tomography (OCT)-based corneal topographic instruments can provide more consistent measurements than the Scheimpflug-based corneal topographers for eyes with advanced keratoconus. More accurate data at the periphery may therefore be obtained by the OCT-based corneal topographer [23, 24].

Another limitation was that we excluded subclinical PMD cases without corneal thinning. Further studies are needed to understand the topographic changes in subclinical PMD, especially for the screening of refractive surgery candidates.

In conclusion, the results of our study show that in our Japanese patient population not only was the crab claw pattern frequently observed in eyes with PMD, but that also in these eyes asymmetric island patterns were frequently present in the anterior and posterior elevation maps and the decentered oval pattern was frequently present in the pachymetric maps. These findings suggest that PMD and keratoconus may not be two non-inflammatory corneal thinning disorders but rather one continuous disorder with different phenotypes. Further research will be necessary to determine the definition of keratoconus and PMD.

Acknowledgments Publication of this article was supported in part by Grant-in-Aid no. 24592669 (to Naoyuki Maeda) for Scientific Research from the Japanese Ministry of the Education, Culture, Sports, Science and Technology. Copy editor: Dr. Duco Hamasaki, Professor Emeritus, Bascom Palmer Eye Institute, University of Miami, Florida.

References

1. Krachmer JH. Pellucid marginal corneal degeneration. Arch Ophthalmol. 1978;96:1217–21.
2. Kayazawa F, Nishimura K, Kodama Y, Tsuji T, Itoi M. Keratoconus with pellucid marginal corneal degeneration. Arch Ophthalmol. 1984;102:895–6.
3. Rodrigues MM, Newsome DA, Krachmer JH, Eiferman RA. Pellucid marginal corneal degeneration: a clinicopathologic study of two cases. Exp Eye Res. 1981;33:277–88.
4. Rabinowitz YS. Keratoconus. Surv Ophthalmol. 1998;42:297–319.
5. Krachmer JH, Feder RS, Belin MW. Keratoconus and related noninflammatory corneal thinning disorders. Surv Ophthalmol. 1984;28:293–322.

6. Gruenauer-Kloevekorn C, Fischer U, Kloevekorn-Norgall K, Duncker GI. Pellucid marginal corneal degeneration: evaluation of the corneal surface and contact lens fitting. Br J Ophthalmol. 2006;90:318–23.
7. Jinabhai A, Radhakrishnan H, O'Donnell C. Pellucid corneal marginal degeneration: a review. Contact Lens Anterior Eye. 2011;34:56–63.
8. Kim KH, Choi SH, Ahn K, Chung ES, Chung TY. Comparison of refractive changes after deep anterior lamellar keratoplasty and penetrating keratoplasty for keratoconus. Jpn J Ophthalmol. 2011;55:93–7.
9. Sridhar MS, Mahesh S, Bansal AK, Nutheti R, Rao GN. Pellucid marginal corneal degeneration. Ophthalmology. 2004;111: 1102–7
10. Walker RN, Khachikian SS, Belin MW. Scheimpflug photographic diagnosis of pellucid marginal degeneration. Cornea. 2008;27:963–6.
11. Ambrósio JR, Klyce SD, Smolek MK, Wilson SE. Pellucid marginal corneal degeneration. J Refract Surg. 2002;18:86–8.
12. Fogla R, Rao SK, Padmanabhan P. Keratectasia in 2 cases with pellucid marginal corneal degeneration after laser in situ keratomileusis. J Cataract Refract Surg. 2003;29:788–91.
13. Ambrósio R Jr, Klyce SD, Wilson SE. Corneal topographic and pachymetric screening of keratorefractive patients. J Refract Surg. 2003;19:24–9.
14. Belin MW, Khachikian SS. Keratoconus. It is hard to define, but.... Am J Ophthalmol. 2007;143:500–3.
15. Belin MW, Asota IM, Ambrosio R Jr, Khachikian SS. What's in a name: keratoconus, pellucid marginal degeneration, and related thinning disorders. Am J Ophthalmol. 2011;152:157–62.
16. Bogan SJ, Waring GO 3rd, Ibrahim O, Drews C, Curtis L. Classification of normal corneal topography based on computer-assisted video keratography. Arch Ophthalmol. 1990;108:945–9.
17. Lee BW, Jurkunas UV, Harissi-Dagher M, Poothullil AM, Tobaigy FM, Azar DT. Ectatic disorders associated with a claw-shaped pattern on corneal topography. Am J Ophthalmol. 2007;144:154–6.
18. Maguire LJ, Klyce SD, McDonald MB, Kaufman HE. Corneal topography of pellucid marginal degeneration. Ophthalmology. 1987;94:519–24.
19. Maeda N, Klyce SD, Tano Y. Detection and classification of mild irregular astigmatism in patients with good visual acuity. Surv Ophthalmol. 1998;43:53–8.
20. Naufal SC, Hess JS, Friedlander MH, Granet NS. Rasterstereography-based classification of normal corneas. J Cataract Refract Surg. 1997;23:222–30.
21. Liu Z, Huang AJ, Pflugfelder SC. Evaluation of corneal thickness and topography in normal eyes using the Orbscan corneal topography system. Br J Ophthalmol. 1999;83:774–8.
22. Saika M, Maeda N, Hirohara Y, Mihashi T, Fujikado T, Nishida K. Four discriminant models for detecting keratoconus pattern using Zernike coefficients of cornea aberrations. Jpn J Ophthalmol. 2013;57:503–9.
23. Nakagawa T, Maeda N, Higashiura R, Hori Y, Inoue T, Nishida K. Corneal topographic analysis in patients with keratoconus using 3-dimensional anterior segment optical coherence tomography. J Cataract Refract Surg. 2011;37:1871–8.
24. Higashiura R, Maeda N, Nakagawa T, Fuchihata M, Koh S, Hori Y, et al. Corneal topographic analysis by 3-dimensional anterior segment optical coherence tomography after endothelial keratoplasty. Invest Ophthalmol Vis Sci. 2012;53:3286–95.

Jpn J Ophthalmol (2014) 58:389–395
DOI 10.1007/s10384-014-0338-0

THE OFFICIAL INTERNATIONAL JOURNAL OF THE JAPANESE OPHTHALMOLOGICAL SOCIETY

CLINICAL INVESTIGATION

Evaluation of corneal epithelial and stromal thickness in keratoconus using spectral-domain optical coherence tomography

Naoyuki Maeda · Tomoya Nakagawa · Ritsuko Higashiura · Mutsumi Fuchihata · Shizuka Koh · Kohji Nishida

Received: 19 January 2014 / Accepted: 3 June 2014 / Published online: 12 July 2014

Abstract
Purpose We sought to assess the corneal thickness of the epithelium and stroma in keratoconic and normal eyes by spectral-domain optical coherence tomography (SD-OCT).
Methods Fifty-seven keratoconic and 20 normal eyes were studied. The eyes were examined by SD-OCT, and the keratoconic eyes were subdivided into 2 groups: those showing only smooth corneal thinning and corneal protrusion on the image (KC1 group) and those showing abnormalities in the Bowman layer or in the stroma, or in both (KC2 group). The thicknesses at the corneal vertex and at the superior, inferior, nasal, and temporal cornea 1.5 mm from the corneal vertex in the KC1 group were compared with those in the normal group. The OCT findings in the KC2 group were described.
Results The epithelial thickness at the corneal vertex and at the inferior and temporal cornea, and the stromal thickness at all points were significantly thinner in the KC1 group than in the normal group ($p < 0.05$). The epithelial and stromal thicknesses at the corneal vertex were significantly correlated in the KC1 group and the normal group ($r^2 = 0.427$, $p < 0.0001$).The epithelial thickness in the KC2 group was not uniform owing to Bowman layer scarring, stromal scars, and secondary corneal amyloidosis.
Conclusions Although epithelial thinning is associated with stromal thinning, when the cornea remains clear, the epithelial thickness may vary because of the irregularity of the stroma beneath the epithelium in patients with keratoconus.

N. Maeda (✉) · T. Nakagawa · R. Higashiura · M. Fuchihata · S. Koh · K. Nishida
Department of Ophthalmology, Osaka University Graduate School of Medicine, Room E7, 2-2 Yamadaoka, Suita, Osaka 565-0871, Japan
e-mail: nmaeda@ophthal.med.osaka-u.ac.jp

Keywords Keratoconus · Spectral-domain optical coherence tomography · Corneal epithelial thickness · Corneal stromal thickness

Introduction

Keratoconus is a corneal disorder characterized by progressive corneal thinning and anterior protrusion of tissue in the central or paracentral region [1, 2]. The pathogenesis of keratoconus is not fully understood, and clarification of its origin will help researchers to develop new treatments and methods to prevent this disease.

Although the opportunity for pathologic examination of keratoconic eyes has been limited mainly to instances of corneal transplantation, several in vivo imaging devices that assess the corneal microstructure have recently been developed. The in vivo confocal microscope has shown some microstructural changes in keratoconic eyes such as lower cell densities of keratocytes and an abnormality in corneal innervation [3–5]. In addition, the high-frequency ultrasound biomicroscope is useful in providing cross-sectional images of the cornea [6]. Reinstein and coworkers have shown that the epithelial thickness profile can be used to improve keratoconus detection by indicating epithelial thinning at the stromal cone [7, 8].

Optical coherence tomography (OCT) was introduced as a noncontact imaging device that provides measurable cross-sectional images of tissues [9]. OCT has been used for the anterior segment of the eye as a complementary examination to the slit-lamp examination for the visualization of nontransparent lesions, observation of tissues with high magnification, and biometry of the anterior segment [10–12].

Epithelial thickness profiles in keratoconus obtained by OCT confirmed apical epithelial thinning [13, 14]. A structural classification of keratoconus (stages 1–5) using 840-nm OCT was recently proposed on the basis of the findings from a large keratoconic population [15].

In this study, cross-sectional images of the cornea in keratoconic eyes were obtained by SD-OCT. The profiles of the epithelial and stromal thicknesses were compared between the normal corneas and those in stage-1 keratoconus, in which apparently normal epithelium and stroma are present at the cone. Furthermore, association between the epithelial and stromal thicknesses was evaluated. In addition, the irregular profiles of corneal epithelia at stage-2 through stage-5 were shown.

Study participants and methods

Study participants

Fifty-seven keratoconic eyes of 39 patients and normal eyes of 20 controls were included in the study. The number of men/women in the keratoconus group was 22/17, and was 10/10 in the control group. The mean (SD) age of the keratoconus group was 37.1 ± 11.7 years, and 34.3 ± 13.2 years in the control group. The groups did not differ significantly in sex ($p = 0.848$, Chi square test) or age ($p = 0.398$, unpaired t test).

The controls had no ocular disorders other than refractive errors; none wore contact lenses. Only one eye of each control participant was used. The criteria for diagnosing keratoconus was the presence of central thinning of the cornea with a Fleischer ring or Vogt striae, or both, detected by slit-lamp examination [16, 17]. Eyes with keratoconus suspect or forme fruste keratoconus were not included.

The institutional review board of Osaka University Hospital approved this study. The research adhered to the tenets of the Declaration of Helsinki. Informed consent was obtained from all participants.

OCT measurement

The eyes were examined by SD-OCT (RTVue, Optovue, Fremont, CA, USA) with a low-magnification cornea lens adapter. The OCT image scan rate of this device is 26,000 A-scans per second, and its vertical resolution is 5 μm. A cross-pattern consisting of vertical and horizontal lines was used, and each line scan consisted of 1024 A-scans over a 6-mm diameter. All scans were centered at the corneal vertex. All participants were examined at least 3 times to confirm the reproducibility of the obtained images, and images with a motion artifact were excluded. We chose the best of the 3 scans of each patient for analysis. To reduce the speckle noise and improve the image quality, the obtained images were averaged from 3 frames with a built-in program.

Qualitative analysis of cross-sectional OCT images

Qualitative analysis of the cross-sectional images was performed for the epithelium, Bowman layer, stromal layer, and posterior surface. On the basis of these findings, the keratoconic eyes were classified into the following two subgroups according to the OCT classification of Sandali and colleagues [15]: stage-1 keratoconic eyes, with clear epithelial and stromal layers, were defined as the KC1 group; stages 2–5 keratoconic eyes, with any abnormal findings other than smooth corneal thinning or corneal protrusion, were defined as the KC2 group.

Quantitative analysis of epithelial and stromal thickness

The epithelial and stromal thicknesses were measured using a built-in measuring tool that corrects the distortions of the images caused by refraction from the anterior corneal surface. The epithelial and stromal thicknesses at the corneal vertex and at the superior, inferior, nasal, and temporal cornea 1.5 mm from the corneal vertex in the KC1 and control groups were measured. Correlation between epithelial thickness and stromal thickness at the corneal vertex was also investigated.

Statistical analysis

Data were analyzed using JMP version 9 software (SAS, Cary, NC, USA). The Chi square test was used to compare the sex ratio of the study participants. The unpaired t test was used to compare the ages of the keratoconus patients and the controls. The Mann–Whitney test was used to compare the epithelial and stromal thicknesses of the KC1 group and the control group. One-way repeated measures analysis of variance (ANOVA) and the Tukey–Kramer test were used to compare the epithelial and stromal thicknesses at the different locations in the KC1 group and the control group. The correlation coefficients between the epithelial and stromal thicknesses at the corneal vertex were calculated using the KC1 group and the control group. A probability value less than 0.05 was considered significant for all analyses.

Results

Qualitative analysis of cross-sectional OCT images

In the controls, four layers of the cornea were distinctly observed by SD-OCT. These layers consisted of the

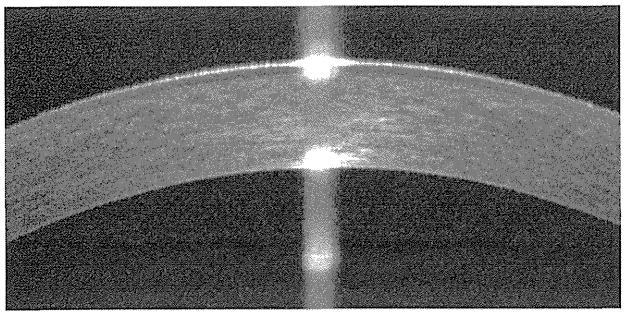

Fig. 1 SD-OCT horizontal image of a normal cornea. The epithelium, Bowman layer, stroma, and Descemet membrane/endothelium complex were distinctly observed

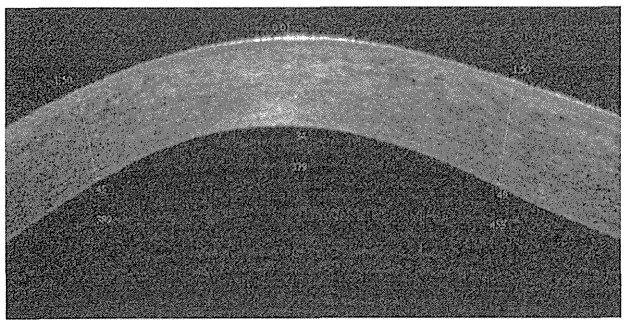

Fig. 2 SD-OCT vertical image of a keratoconic cornea in the KC1 group. SD-OCT did not show microstructural abnormalities within each layer but only smooth thinning of the corneal epithelium and stroma in the central zone and corneal anterior protrusion

epithelium, the Bowman layer, the stroma, and the Descemet membrane/endothelium complex (Fig. 1). No layered structure within the epithelial layer was observed without thinning or thickening. The Bowman layer was recognized as double parallel lines and did not show any hyperreflective abnormalities between the lines. The structure in the stromal layer usually showed a regular pattern of parallel hyperreflective dots and lines without stromal thinning and irregular hyperreflective abnormalities. The Descemet membrane and the endothelium could not be observed as individual layers, and the corneal posterior surface showed a smooth and arch-like configuration.

Thirty of the keratoconic eyes (52.6 %) were classified into the KC1 group, in which the eyes had only smooth corneal thinning and corneal protrusion. These eyes could be distinguished from normal eyes only by abnormality in the corneal thickness profile or in the contours of the anterior and posterior surfaces, or in both. Microstructural abnormality was not observed in the epithelium, the Bowman layer, the stroma, or the Descemet membrane/endothelium complex in the KC1 group (Fig. 2), although the images of the Bowman layer were not clear in the keratoconic eyes when compared with those in the control eyes.

Twenty-seven of the keratoconic eyes (47.4 %) were classified into the KC2 group. In 21 eyes (36.8 %), hyperreflective abnormalities were observed in the Bowman layer or in the anterior stroma, or in both. These eyes with hyperreflective abnormalities at the Bowman layer level were considered to have stage-2 keratoconus, and those with posterior displacement of the hyperreflective structures, to have stage-3 keratoconus. Slit-lamp examination revealed subepithelial reticular haze or corneal stromal scars, or both, in these high-intensity areas. The SD-OCT images showed varied depths of the hyperreflective abnormalities. The high-intensity areas were located in the subepithelial stroma in some cases, and extended to the deep stroma in other cases (Fig. 3, top left and right). Although irregular interfaces between the epithelium and stroma were observed in 12 eyes (21 %), the epithelial surfaces appeared fairly smooth even in those eyes. The epithelial thickness was not uniform and was sometimes thick on one stromal opacity and thin on another.

A remarkable abnormal microstructure within the epithelial layer was observed in only 2 eyes (3.5 %) of the KC2 group; in these 2 eyes, irregularly elevated lesions with high intensity were observed (Fig. 3, bottom left). Slit-lamp examination showed that these elevated lesions were caused by secondary corneal amyloidosis [18].

Irregular corneal posterior surfaces with deep stromal scars were observed in 4 eyes (7.0 %) of the KC2 group (Fig. 3, bottom right). These findings corresponded with stage-5b keratoconus, in which the stromal scar is located in the posterior surface owing to rupture of the Descemet membrane. All of these 4 eyes had a history of acute corneal hydrops.

Quantitative analysis of epithelial and stromal thickness

The respective average thicknesses (μm) of the corneal epithelium/stroma at the corneal vertex and superior, inferior, nasal, and temporal cornea were 58.3/473.8, 56.2/493.3, 56.4/467.3, 55.0/471.4, and 54.6/486.6 in the control group and 42.8/403.1, 55.1/449.3, 49.3/396.8, 48.1/402.2, and 55.0/435.5 in the KC1 group (Figs. 4, 5). The stromal thicknesses at all of the points and the epithelial thicknesses at the corneal vertex and the inferior and temporal cornea were significantly thinner in the KC1 group than those in the control group (Mann-Whitney test).

In the controls, one-way repeated measures ANOVA revealed no significant differences in the epithelial thickness among the measured points ($p = 0.1932$). However, it did reveal a significant difference in the stromal thickness among the measured points ($p = 0.0137$). The Tukey–

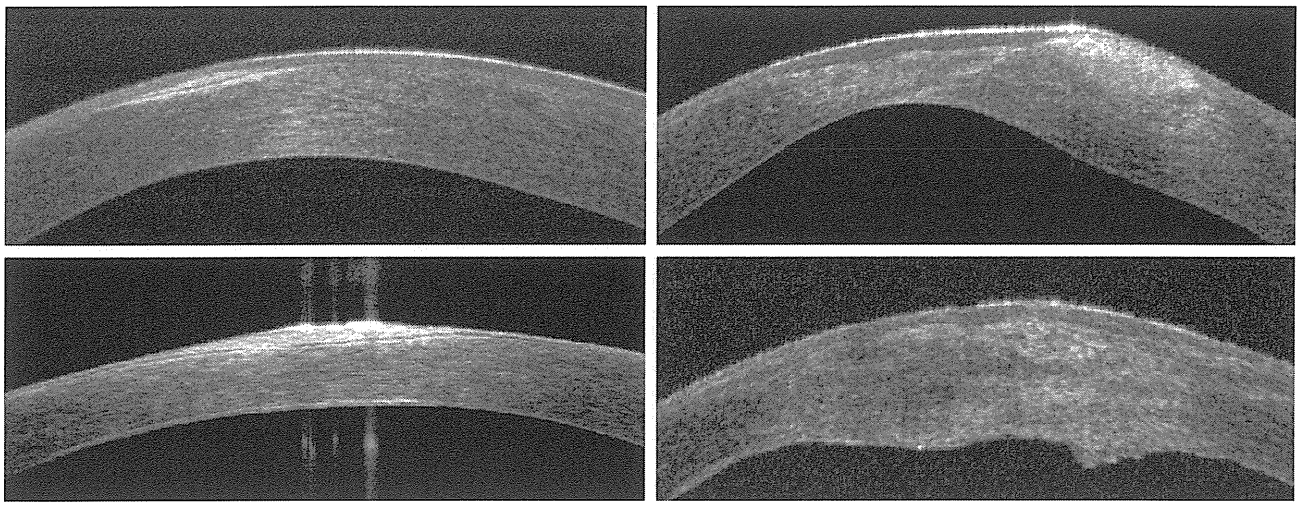

Fig. 3 SD-OCT vertical images of keratoconic corneas in the KC2 group. High-intensity areas were observed in the subepithelial stroma in some cases (*top left*, stage-2) and in the deep stroma in other cases (*top right*, stage-3). Irregularly elevated lesions with high intensity because of corneal deposits were observed (*bottom left*). Irregular corneal posterior surfaces were observed in eyes with histories of acute hydrops (*bottom right*, stage-5b). The interface between the epithelium and stroma showed complex shapes in some eyes. The distribution of the epithelial thickness was variable and the shape of the precorneal tearfilm was relatively smooth because of the compensational effect of the epithelium

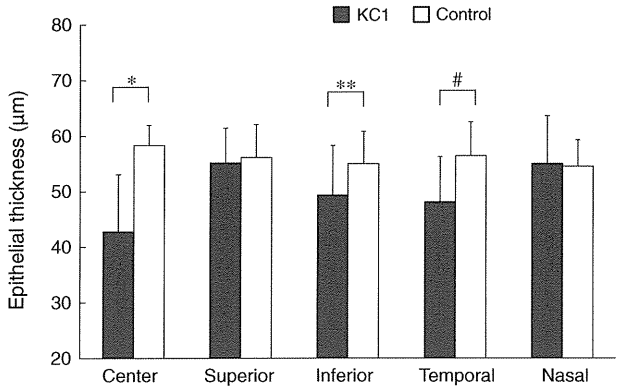

Fig. 4 Average thicknesses (μm) of the corneal epithelium at the corneal vertex and superior, inferior, nasal, and temporal cornea. The epithelial thicknesses in the center, inferior, and temporal regions of the keratoconic cornea (KC1) were significantly thinner than those of the normal cornea ($*p < 0.001$, $**p = 0.0110$, $\#p = 0.0005$), but were not significantly different in the superior ($p = 0.5985$) and nasal ($p = 0.6229$) regions. One-way repeated measures ANOVA revealed no significant differences in the epithelial thickness among the measured points in the normal controls ($p = 0.1932$), but there was a significant difference in the epithelial thickness among the measured points in the KC1 group ($p < 0.001$)

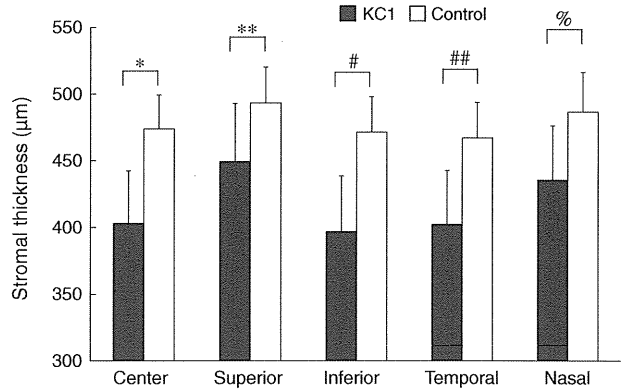

Fig. 5 Average thicknesses (μm) of the corneal stroma at the corneal vertex and superior, inferior, nasal, and temporal cornea. The stromal thicknesses at all the points ($*p < 0.001$, $**p = 0.0003$, $^{\#}p < 0.0001$, $^{\#\#}p < 0.0001$, $^{\%}p < 0.0001$) were significantly thinner in the KC1 group than in the control group. Significant differences were revealed in stromal thickness among the measured points in the control group ($p = 0.0137$) and KC1 group ($p < 0.001$)

Kramer test indicated that the stromal thickness in the superior region was significantly thicker than that in the temporal region ($p = 0.0243$).

In the KC1 group, one-way repeated measures ANOVA revealed a significant difference in the epithelial thickness among the measured points ($p < 0.001$). The Tukey–Kramer test indicated that the epithelial thickness in the central region was significantly thinner than those in the superior ($p < 0.0001$), nasal ($p < 0.0001$), and inferior ($p = 0.0289$) regions. The epithelial thickness in the temporal region was significantly thinner than those in the superior ($p = 0.0155$) and nasal ($p = 0.0178$) regions. In addition, one-way repeated measures ANOVA revealed a significant difference in the stromal thickness among the measured points ($p < 0.001$). The Tukey–Kramer test indicated that the stromal thickness in the inferior region was significantly thinner than those in the superior

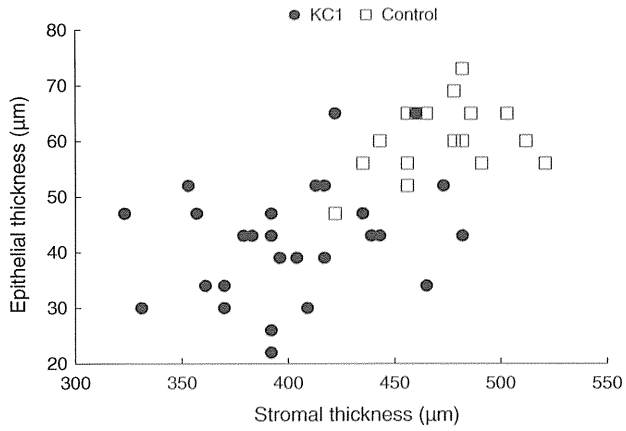

Fig. 6 Correlation between epithelial and stromal thicknesses at the corneal vertex in the control and KC1 groups. The correlation coefficients were not significant in the control eyes ($r^2 = 0.097$, $p = 0.18$) but were significant in the KC1 group ($r^2 = 0.194$, $p = 0.008$)

($P < 0.0001$) and nasal ($P = 0.0034$) regions, and that the stromal thickness in the temporal region was thinner than those in the superior ($p = 0.0002$) and nasal ($p = 0.0177$) regions. The stromal thickness in the central region was significantly thinner than those in the superior ($p = 0.0002$) and nasal ($p = 0.0223$) regions.

The epithelial and stromal thicknesses at the corneal vertex were significantly correlated ($r^2 = 0.4272$, $p < 0.0001$; Fig. 6).

Discussion

Qualitative analysis of cross-sectional OCT images

In this study, SD-OCT showed the detailed corneal microstructure, as previously described [13–15], and permitted separate evaluation of the epithelium and stroma in all study participants.

Corrections for OCT image distortions caused by refraction of the anterior surface are needed for precise measurement of corneal thickness [19]. Because the RTVue system automatically delineated the anterior and posterior corneal boundaries and corrected those distortions, corneal thickness was assessed without difficulty in this study. Because the change in the corneal refractive index due to corneal histopathologic abnormalities may affect the measurements, the validity of the measurement results for abnormal corneas must be carefully assessed [20].

The tear film layer could not be clearly distinguished from the epithelial layer by SD-OCT. Some previous studies reported that the central tear film thickness was approximately 3 μm [21–23], which was smaller than the resolution of the SD-OCT. The central epithelial thickness measured by very high-frequency digital ultrasound or confocal microscopy was thinner than that in this study, probably because the tear film was not incorporated in the epithelial thickness with those devices. However, the epithelial thickness measured in this study may include the tear film thickness.

The hyperreflective abnormalities in the Bowman layer or corneal stromal layer, or in both, observed in the KC2 group were found at the corneal opacities. In addition to corneal aberration caused by irregular corneal shape, the scattering caused by the corneal opacity can be an important factor affecting the visual performance of keratoconic eyes. Quantification of this scattering of the cornea might be possible with OCT.

One of the interesting findings in the KC2 group was the variation in the epithelial thickness profile. Some eyes showed compensatory epithelial thickening in the stromal scar. This finding was consistent with those of previous reports in which OCT [13, 14] or light microscopy [24, 25] was used. In addition, as shown in Fig. 3, epithelial thinning was observed even on the stromal scar or on the secondary corneal amyloidosis. This finding suggested that the variations in the profile of epithelial thickness were due not to the stromal pathology but to the shape of the anterior surface of the corneal stroma. The contour of the anterior surface of the corneal epithelium on the OCT image, i.e., the shape of the precorneal tear film, was smoother than that of the anterior stroma for most of the eyes. Epithelial thickening and thinning probably play a role in the reduction of the corneal aberrations due to irregularity of the anterior surface of the stroma by creating smoother contours of the anterior epithelial surface. Because the refractive indices of the corneal epithelium and stroma are different [26, 27], refraction at the irregular interface between them may cause part of the corneal aberrations.

Quantitative analysis of epithelial and stromal thicknesses

The central epithelial thickness in the normal eyes measured in this study was similar or slightly thicker than in previous studies using OCT [13, 14, 28–33]. Because international variations in the normative elevation map obtained by Scheimpflug-based corneal tomography are known [34], it may be interesting to investigate the international differences in the central epithelial thickness in a normal population.

Reinstein and colleagues reported that the corneal epithelium was thicker inferiorly than superiorly [35]. Haque and colleagues reported that peripheral epithelial thickness

was thickest in the superior region and thinnest in the inferior region [32]. In the current study, no difference in the epithelial thicknesses of the normal eyes was observed among the measured locations in the central 3-mm diameter. Further studies are needed to determine the differences in the normal epithelial thickness according to corneal location by including more study participants and checking the peripheral cornea by use of epithelial mapping.

It was already reported that both the corneal thickness and the epithelial thickness in keratoconic eyes was thinnest in the inferior temporal quadrant [13, 15, 32, 33]. Our findings are consistent with these previous findings.

The current study is the first to show positive correlations between the epithelial and stromal thicknesses at the corneal vertex in a KC1 group and normal controls.

Why the epithelial thickness and stromal thickness were positively correlated is unclear. One possible reason is that the proportion of the epithelial thickness to the stromal thickness is constant; another is that the shape of the anterior stromal surface differs between eyes with a thin stroma and eyes with a thick stroma. Epithelial thinning may compensate for the localized anterior protrusion of the cornea due to stromal thinning in keratoconus [7, 15]. Superficial punctate keratopathy is sometimes seen in the area of stromal thinning in keratoconus, even in patients who do not wear rigid gas-permeable contact lenses. This may be caused by the fragility of the superficial cells in the thinned corneal epithelial layer overlying the thinning stromal area.

It would be interesting to investigate the relationship between higher-order aberrations due to anterior stromal surface and corneal epithelial thinning.

We recently showed the topographic pattern of keratoconus in an anterior elevation map obtained with a Scheimpflug-based corneal tomographer. The results indicated a wide variety of patterns, including asymmetric island (37 %), asymmetric regular ridge (24 %), asymmetric in complete ridge (16 %), and central island (12 %) patterns [36]. It may be interesting to investigate the correlation between the anterior elevation map and the epithelial map.

Limitations of the current study

The current study has some limitations. The number of study participants in this retrospective study was small, and the OCT measurements were limited to the central 3-mm zone of the cornea for both the vertical and the horizontal directions. A detailed assessment of corneal epithelial thickness mapping including the peripheral zone in a large prospective study will be necessary.

Our study may have included some effects of contact-lens wearing on corneal thickness. Although it is preferable for patients to stop wearing rigid gas-permeable contact lenses before an examination to avoid such effects, it is difficult for patients with keratoconus to stop wearing these lenses for long periods before eye examinations.

The usefulness of topographic analysis of the corneal epithelium by SD-OCT in diagnosing keratoconus was recently presented [13]. Further studies using individuals with keratoconus suspect or forme fruste keratoconus will be necessary to develop a clinically useful screening system for avoiding keratectasia after LASIK. Comparison of the screening abilities of the corneal topographer and the aberrometer, and epithelial mapping with OCT in the early stages of keratoconus will reveal the most sensitive and most specific modality to detect this condition.

Acknowledgments Publication of this article was supported in part by Grant-in-Aid no. 24592669 for Scientific Research (to N.M.) from the Japanese Ministry of the Education, Culture, Sports, Science, and Technology. The authors would like to thank Enago (www.enago.jp) for the English language review.

Conflicts of interest N. Maeda, Research grant (Topcon Corporation); T. Nakagawa, None; R. Higashiura, None; M Fuchihata, None; S. Koh, None; K. Nishida, Consultant fees (Alcon Japan, Otsuka Pharmaceutical).

REFERENCES

1. Krachmer JH, Feder RS, Belin MW. Keratoconus and related noninflammatory corneal thinning disorders. Surv Ophthalmol. 1984;28:293–322.
2. Rabinowitz YS. Keratoconus. Surv Ophthalmol. 1998;42: 297–319.
3. Erie JC, Patel SV, McLaren JW, Nau CB, Hodge DO, Bourne WM. Keratocyte density in keratoconus: a confocal microscopy study(a). Am J Ophthalmol. 2002;134:689–95.
4. Ku JY, Niederer RL, Patel DV, Sherwin T, McGhee CN. Laser scanning in vivo confocal analysis of keratocyte density in keratoconus. Ophthalmology. 2008;115:845–50.
5. Niederer RL, Perumal D, Sherwin T, McGhee CN. Laser scanning in vivo confocal microscopy reveals reduced innervation and reduction in cell density in all layers of the keratoconic cornea. Invest Ophthalmol Vis Sci. 2008;49:2964–70.
6. Reinstein DZ, Silverman RH, Rondeau MJ, Coleman DJ. Epithelial and corneal thickness measurements by high-frequency ultrasound digital signal processing. Ophthalmology. 1994;101:140–6.
7. Reinstein DZ, Archer TJ, Gobbe M. Corneal epithelial thickness profile in the diagnosis of keratoconus. J Refract Surg. 2009;25: 604–10.
8. Reinstein DZ, Gobbe M, Archer TJ, Silverman RH, Coleman DJ. Epithelial, stromal, and total corneal thickness in keratoconus: three-dimensional display with artemis very-high frequency digital ultrasound. J Refract Surg. 2010;26:259–71.
9. Huang D, Swanson EA, Lin CP, Schuman JS, Stinson WG, Chang W, et al. Optical coherence tomography. Science. 1991;254:1178–81.
10. Izatt JA, Hee MR, Swanson EA, Lin CP, Huang D, Schuman JS, et al. Micrometer-scale resolution imaging of the anterior eye

in vivo with optical coherence tomography. Arch Ophthalmol. 1994;112:1584–9.
11. Ramos JL, Li Y, Huang D. Clinical and research applications of anterior segment optical coherence tomography: a review. Clin Experiment Ophthalmol. 2009;37:81–9.
12. Maeda N. Optical coherence tomography for corneal diseases. Eye Contact Lens. 2010;36:254–9.
13. Li Y, Tan O, Brass R, Weiss JL, Huang D. Corneal epithelial thickness mapping by Fourier-domain optical coherence tomography in normal and keratoconic eyes. Ophthalmology. 2012;119: 2425–33.
14. Rocha KM, Perez-Straziota CE, Stulting RD, Randleman JB. SD-OCT analysis of regional epithelial thickness profiles in keratoconus, postoperative corneal ectasia, and normal eyes. J Refract Surg. 2013;29:173–9.
15. Sandali O, El Sanharawi M, Temstet C, Hamiche T, Galan A, Ghouali W, et al. Fourier-domain optical coherence tomography imaging in keratoconus: a corneal structural classification. Ophthalmology. 2013;120:2403–12.
16. Maeda N, Klyce SD, Smolek MK, Thompson HW. Automated keratoconus screening with corneal topography analysis. Invest Ophthalmol Vis Sci. 1994;35:2749–57.
17. Maeda N, Fujikado T, Kuroda T, Mihashi T, Hirohara Y, Nishida K, et al. Wavefront aberrations measured with Hartmann-Shack sensor in patients with keratoconus. Ophthalmology. 2002;109:1996–2003.
18. Araki-Sasaki K, Hirano K, Osakabe Y, Kuroda M, Kitagawa K, Mishima H, et al. Classification of secondary corneal amyloidosis and involvement of lactoferrin. Ophthalmology. 2013;120:1166–72.
19. Mohamed S, Lee GK, Rao SK, Wong AL, Cheng AC, Li EY, et al. Repeatability and reproducibility of pachymetric mapping with Visante anterior segment-optical coherence tomography. Invest Ophthalmol Vis Sci. 2007;48:5499–504.
20. Wang J, Fonn D, Simpson TL, Jones L. Relation between optical coherence tomography and optical pachymetry measurements of corneal swelling induced by hypoxia. Am J Ophthalmol. 2002;134:93–8.
21. King-Smith PE, Fink BA, Fogt N, Nichols KK, Hill RM, Wilson GS. The thickness of the human precorneal tear film: evidence from reflection spectra. Invest Ophthalmol Vis Sci. 2000;41: 3348–59.
22. Wang J, Fonn D, Simpson TL, Jones L. Precorneal and pre- and postlens tear film thickness measured indirectly with optical coherence tomography. Invest Ophthalmol Vis Sci. 2003;44:2524–8.
23. Wang J, Aquavella J, Palakuru J, Chung S, Feng C. Relationships between central tear film thickness and tear menisci of the upper and lower eyelids. Invest Ophthalmol Vis Sci. 2006;47:4349–55.
24. Scroggs MW, Proia AD. Histopathological variation in keratoconus. Cornea. 1992;11:553–9.
25. Eagle RCJr, Dillon EC, Laibson PR. Compensatory epithelial hyperplasia in human corneal disease. Trans Am Ophthalmol Soc. 1992;90:265–73.
26. Patel S, Marshall J, Fitzke FWIII. Refractive index of the human corneal epithelium and stroma. J Refract Surg. 1995;11:100–5.
27. Simon G, Ren Q, Kervick GN, Parel JM. Optics of the corneal epithelium. Refract Corneal Surg. 1993;9:42–50.
28. Wang J, Thomas J, Cox I, Rollins A. Noncontact measurements of central corneal epithelial and flap thickness after laser in situ keratomileusis. Invest Ophthalmol Vis Sci. 2004;45:1812–6.
29. Sin S, Simpson TL. The repeatability of corneal and corneal epithelial thickness measurements using optical coherence tomography. Optom Vis Sci. 2006;83:360–5.
30. Tao A, Wang J, Chen Q, Shen M, Lu F, Dubovy SR, et al. Topographic thickness of Bowman's layer determined by ultra-high resolution spectral domain-optical coherence tomography. Invest Ophthalmol Vis Sci. 2011;52:3901–7.
31. Francoz M, Karamoko I, Baudouin C, Labbe A. Ocular surface epithelial thickness evaluation with spectral-domain optical coherence tomography. Invest Ophthalmol Vis Sci. 2011;52:9116–23.
32. Haque S, Jones L, Simpson T. Thickness mapping of the cornea and epithelium using optical coherence tomography. Optom Vis Sci. 2008;85:E963–76.
33. Zhou W, Stojanovic A. Comparison of corneal epithelial and stromal thickness distributions between eyes with keratoconus and healthy eyes with corneal astigmatism $\geq$ 2.0 D. PLoS ONE. 2014;9:e85994.
34. Feng MT, Belin MW, Ambrósio R Jr, Grewal SP, Yan W, Shaheen MS, et al. International values of corneal elevation in normal subjects by rotating Scheimpflug camera. J Cataract Refract Surg. 2011;37:1817–21.
35. Reinstein DZ, Archer TJ, Gobbe M, Silverman RH, Coleman DJ. Epithelial thickness in the normal cornea: three-dimensional display with Artemis very high-frequency digital ultrasound. J Refract Surg. 2008;24:571–81.
36. Fuchihata M, Maeda N, Toda R, Koh S, Fujikado T, Nishida K. Characteristics of corneal topographic and pachymetric patterns in patients with pellucid marginal corneal degeneration. Jpn J Ophthalmol. 2014;58:131–8.

Higher-Order Aberrations of Anterior and Posterior Corneal Surfaces in Patients With Keratectasia After LASIK

Naoyuki Maeda,[1] Tomoya Nakagawa,[1] Ryo Kosaki,[1] Shizuka Koh,[1] Makoto Saika,[2] Takashi Fujikado,[3] and Kohji Nishida[1]

[1]Department of Ophthalmology, Osaka University Graduate School of Medicine, Osaka, Japan
[2]Research Institute, Optics Laboratory, Topcon Corporation, Tokyo, Japan
[3]Department of Applied Visual Science, Osaka University Graduate School of Medicine, Osaka, Japan

Correspondence: Naoyuki Maeda, Department of Ophthalmology, Osaka University Graduate School of Medicine Room E7, 2-2 Yamadaoka, Suita, 565-0871, Japan; nmaeda@ophthal.med.osaka-u.ac.jp.

Submitted: March 19, 2014
Accepted: May 16, 2014

Citation: Maeda N, Nakagawa T, Kosaki R, et al. Higher-order aberrations of anterior and posterior corneal surfaces in patients with keratectasia after LASIK. *Invest Ophthalmol Vis Sci.* 2014;55:3905–3911. DOI:10.1167/iovs.14-14391

Purpose. We investigated higher-order aberrations (HOAs) of the anterior and posterior corneal surfaces in patients with keratectasia after LASIK.

Methods. The subjects comprised four groups: 12 eyes with keratectasia after LASIK, 30 eyes following LASIK without keratectasia, 30 keratoconic eyes, and 30 normal eyes. Corneal HOAs due to the anterior and posterior corneal surfaces for 6-mm pupils (root mean square [μm]) were obtained using a Scheimpflug-based corneal tomographer and compared among the four groups.

Results. There were significant differences in total HOAs of the anterior and posterior corneal surfaces (mean ± SD) in the keratectasia (2.49 ± 1.37 and 0.83 ± 0.57), keratoconus (4.50 ± 2.57 and 1.18 ± 0.65), LASIK (0.84 ± 0.25 and 0.14 ± 0.04), and normal (0.52 ± 0.15 and 0.17 ± 0.06) groups except for between keratoconus and keratectasia at the posterior surface. Keratectasia and keratoconus showed similar coma-dominant patterns at both surfaces, and there were no significant differences in the Zernike terms between both groups except for the total HOAs and coma aberration at the anterior surface.

Conclusions. Although flap creation and laser ablation were supposed to center on the primary line of sight in LASIK, keratectasia after LASIK showed coma-dominant HOAs at both corneal surfaces. This suggests that the cornea in keratectasia has optical properties similar to those in keratoconus.

Keywords: keratectasia, LASIK, keratoconus, aberration, cornea

LASIK has been the primary type of corneal refractive surgery for mild-to-moderate myopia and myopic astigmatism for many years. The efficacy and safety of LASIK have been excellent, and have been improved with the aid of wavefront technology and the femtosecond laser.[1–3] However, there still may be some intraoperative and postoperative complications following LASIK.

Keratectasia or post-LASIK corneal ectasia, is a serious complication after LASIK.[4–8] Keratectasia can be defined as a progressive anterior protrusion of the central cornea after corneal refractive surgery with steepening and irregularity of the corneal shape inside the optical zone. This condition induces the progression of myopic astigmatism and irregular astigmatism that can lead to the loss of uncorrected distance visual acuity and corrected distance visual acuity (CDVA).

Although the mechanism of keratectasia still is unknown, there are at least two pathogenesis for keratectasia; that is, a thin stromal bed with normal stroma[4,6] or a sufficient stromal bed with undetected or mild keratoconus.[5] Histopathologic studies have revealed the consistent or discrepant results for the similarities between keratoconus and keratectasia.[9–11]

We investigated the higher-order aberrations (HOAs) of the anterior and posterior corneal surfaces in eyes with keratectasia after LASIK using a rotating Scheimpflug corneal tomographer, and we compared those measurements with those in the eyes in the normal, LASIK, and keratoconus groups.

Methods

This retrospective, observational case series included 12 eyes of 7 cases that had LASIK in other clinics and were referred to the Osaka University Hospital as having keratectasia after LASIK (Table 1). We included as the subjects 30 eyes without keratectasia after LASIK, 30 keratoconic eyes, and 30 normal eyes (Table 1).

Keratectasia was defined as the progressive anterior protrusion of the central cornea after LASIK with the loss of CDVA. Normal eyes (control) had no ocular disorders except for refractive errors. The criteria for diagnosing keratoconus were the presence of central thinning of the cornea with a Fleischer ring and/or Vogt's striae by slit-lamp examination.[12] Eyes that were keratoconus suspect or had forme fruste keratoconus were not included. Keratoconic eyes with corneal scarring and a history of acute hydrops or other disorders that affected the topographic findings also were excluded. All eyes were diagnosed by one experienced ophthalmologist (NM).

The research followed the tenets of the Declaration of Helsinki. Informed consent was obtained from the subjects after explanation of the nature and possible consequences of the study. The research was approved by the Institutional Review Board of Osaka University.

The subjects were examined using a rotating Scheimpflug camera (PentacamHR; Oculus Optikgeräte, GmbH, Wetzlar,

Table 1. Subject Data

	Cases/Eyes	Male/Female	R/L	Age
Control	30/30	16/14	16/14	38.9 ± 12.8
LASIK	15/30	6/9	15/15	38.9 ± 10.7
Keratoconus	30/30	15/15	15/15	33.6 ± 9.0
Keratectasia	7/12	4/3	6/6	39.1 ± 9.7

Germany). A total of 25 pictures was taken during one scan to reconstruct a three-dimensional model of the entire corneal configuration. All subjects were examined at least twice to confirm the reproducibility of the obtained data. The quality of the data from examination was accessed with a built-in program, and the results with serious errors were excluded.

To maintain the consistency of the methodology in our study, HOAs of 6-mm pupils were calculated by an original program for the anterior and posterior corneal surfaces as published previously.[13,14] The wavefront aberration was expanded with the normalized Zernike polynomials. For each pair of the standard Zernike terms for trefoil, coma, tetrafoil, and secondary astigmatism, a combined value for the magnitude and axis was calculated for the anterior and posterior corneal aberrations. Total HOAs were defined as the root mean square of the magnitudes for the third- and fourth-order aberrations. The magnitude of the spherical aberration was expressed as either a positive or negative value and not as an absolute value. The axes of left eyes were transposed about the vertical axis to correct for enantiomorphism.[15]

The data were analyzed using statistical analysis software JMP version 9 (SAS, Inc., Cary, NC, USA). The Kruskal-Wallis test was used to compare the total HOAs, trefoil, coma, tetrafoil, secondary astigmatism, and spherical aberration of the anterior and posterior corneal surfaces among the four groups. The Kruskal-Wallis test also was used to compare the ratios of the anterior corneal HOAs to the posterior corneal HOAs (A/P ratio) for total HOAs and each Zernike term except for spherical aberration among the four groups. The Steel-Dwass method was used for pair comparisons. P values of <0.05 were considered statistically significant.

Results

Figure 1 shows the characteristic examples of elevation and HOA maps for the anterior and posterior surfaces in the normal eye, post-LASIK eye, keratectasia eye, and keratoconic eye.

The HOA maps caused by anterior/posterior corneal surfaces in the normal eye (column 1) showed a flat wavefront. The HOA map of the anterior surface in the post-LASIK eye (column 2) revealed a slightly decentered fast wavefront that was associated with the central depression pattern in the anterior elevation map. Keratectasia (column 3) and keratoconic (column 4) eyes showed a vertical coma pattern in the anterior and posterior HOA maps. The HOAs from the posterior surface were smaller, and the pattern was in the opposite direction than HOAs from the anterior surface. The means and the standard deviations of the total HOAs and each Zernike term for the anterior and posterior corneal surfaces inside the 6-mm diameter are shown in Figures 2 and 3, respectively.

The Kruskal-Wallis test showed that the total HOAs and each Zernike term for the anterior and posterior corneal surfaces were significantly different among the four groups ($P < 0.0001$), and there were significant differences in the A/P ratio of the total HOAs ($P < 0.0001$), coma ($P = 0.0005$), trefoil ($P = 0.0215$), and secondary astigmatism ($P < 0.0001$), but no significant difference in tetrafoil ($P = 0.90084$).

The results of statistical significances between two groups with the Steel-Dwass method are shown in Table 2. There were significant differences in the total HOAs of the anterior and posterior corneal surfaces (mean ± SD) among the keratectasia (2.49 ± 1.37 and 0.83 ± 0.57), keratoconus (4.50 ± 2.57 and 1.18 ± 0.65), LASIK (0.84 ± 0.25 and 0.14 ± 0.04), and normal (0.52 ± 0.15 and 0.17 ± 0.06) groups except between keratoconus and keratectasia at the posterior surface.

Keratectasia and keratoconus showed a similar coma-dominant pattern in the Zernike terms of both surfaces. No significant differences in the total HOAs and all Zernike terms for the anterior and posterior surfaces were found between keratoconus and keratectasia except for the total HOAs and coma at the anterior surface.

In the comparison between normal and post-LASIK eyes, the total HOAs, coma, and spherical aberration at the anterior surface in the LASIK group were significantly higher than those in the normal controls, and the total HOAs and secondary astigmatism at the posterior surface in the LASIK group were significantly lower than those in normal eyes. There were no significant differences between both groups except these parameters.

There were significant differences in the total HOAs and all Zernike terms of the anterior and posterior surfaces between keratoconic and normal eyes, and between keratoconic and post-LASIK eyes except tetrafoil at both surfaces. There also were significant differences in the total HOA, trefoil, coma, and secondary astigmatism of the anterior and posterior surfaces between keratectasia and normal eyes, and between keratectasia and post-LASIK eyes.

Figure 4 shows the A/P ratios for the total HOAs and each Zernike term. The total HOAs of the anterior surfaces were approximately 3 to 4 times greater than those of the posterior surfaces in control eyes. The A/P ratio for the total HOAs in LASIK eyes was significantly higher than that in normal, keratoconic, and keratectasia eyes. The A/P ratio of coma in LASIK eyes also was significantly higher than that in normal eyes.

Figure 5 indicates the coma due to the anterior and posterior surfaces on the polar coordinates. The scatter patterns in keratectasia and keratoconus were similar for the anterior and posterior surfaces. The axes in most of keratectasia and keratoconic eyes were distributed from 45° to 90° for the anterior surface, but the axes were distributed from 180° to 270° in the opposite direction for the posterior surface. In contrast, the axis of the coma of the anterior and posterior surfaces in normal and post-LASIK eyes was small, and no such trend was seen for the axis of coma of the anterior and posterior surfaces.

Discussion

It will be important to understand the characteristics of the optical properties of the anterior and posterior corneal surfaces in keratectasia to improve the results of treatments for keratectasia, such as prescribing rigid gas permeable (RGP) contact lenses,[16,17] intracorneal rings,[18] corneal crosslinking,[19] and corneal transplantation. Only few studies have been conducted for the evaluation of HOAs in keratectasia.[20,21] Keratectasia and post-LASIK eyes were compared in one study; the coma-like aberrations and spherical-like aberrations that were calculated based on the anterior corneal shape were significantly higher in keratectasia eyes than in post-LASIK eyes.[21] Another study showed an increase in ocular HOAs and

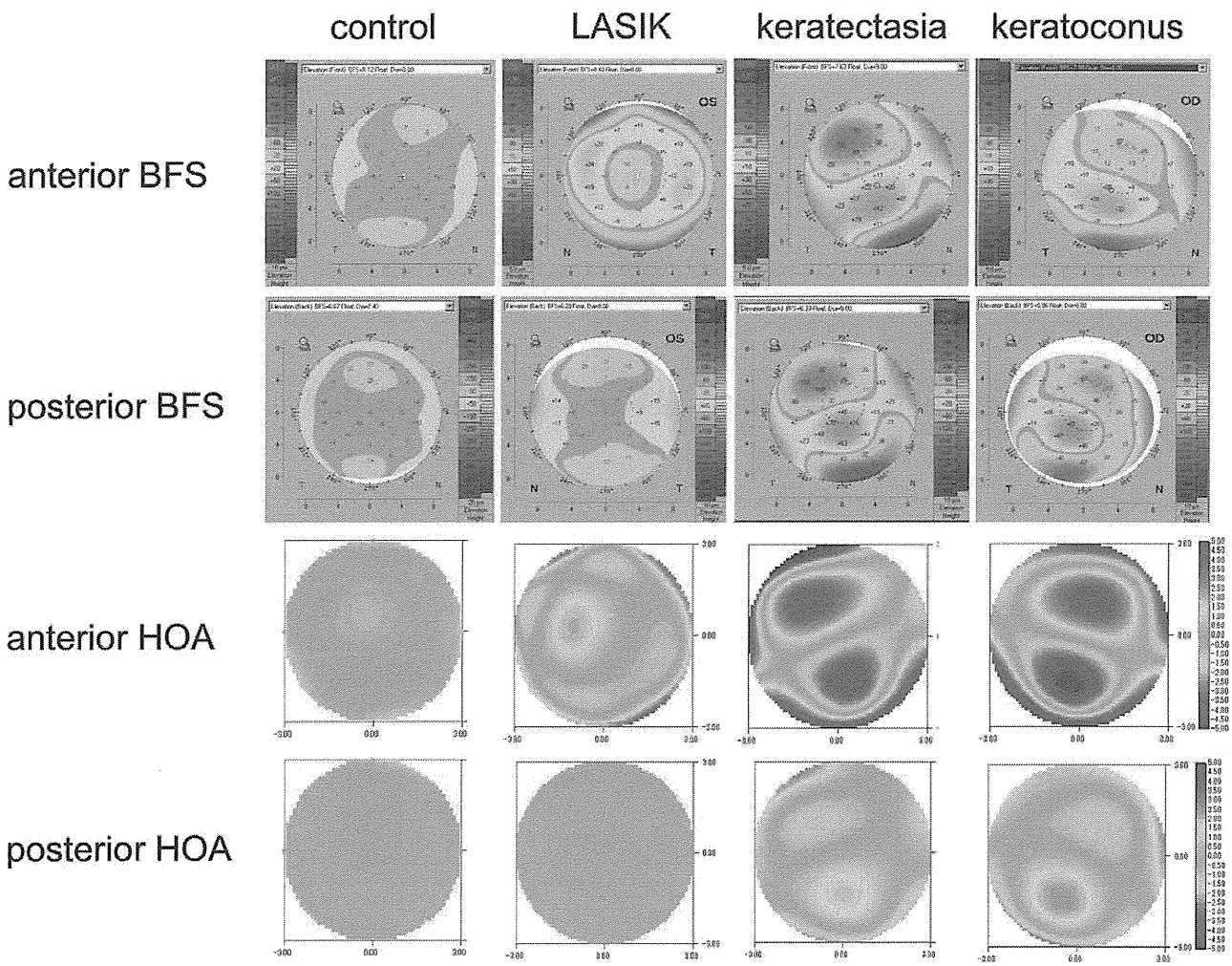

FIGURE 1. The characteristic examples of elevation and HOA maps of the anterior and posterior surfaces in normal, post-LASIK, keratectasia, and keratoconic eyes. No clinically relevant HOAs were detected for the anterior and posterior surfaces in control eyes (*column 1*). The HOA map of the anterior surface in post-LASIK eyes (*column 2*) revealed a slightly decentered fast wavefront pattern (*warmer colors*) that was associated with the central depression pattern in the anterior elevation map associated with laser ablation. Keratectasia (*column 3*) and keratoconic (*column 4*) eyes showed an anterior protrusion at the paracentral zone in the anterior and posterior elevation maps. These changes yielded the vertical coma pattern in the anterior and posterior HOA maps. The amplitude of HOAs from the posterior surface was smaller, and the pattern of the maps was in the opposite direction than those from the anterior surface in keratoconus and keratectasia. An inferior slow pattern; that is, a pattern in which the slow wavefront area (*cooler colors*) was located at the inferior area, was seen for the HOA maps of the anterior surface. The HOA maps from the posterior surface were in the opposite direction; that is, a superior slow pattern, compared to the anterior surface in keratoconic and keratectasia eyes. BFS, best-fit-sphere.

an increase in higher order irregularity for the elevations of the anterior and posterior surfaces.[20]

The results of the present study confirmed the same trend for an increase in HOAs at the anterior corneal surface. In addition, the increase in HOAs at the posterior corneal surface and the details of the Zernike terms for both surfaces were described.

It is believed that these HOAs in keratectasia may be caused by the combination of laser ablation to the stromal bed and the protrusions of the anterior and posterior corneal surfaces associated with the biomechanical weakness of the cornea.

Post-LASIK eyes had slightly higher HOAs at the anterior corneal surface and normal HOAs at the posterior surface, resulting in the increase of the A/P ratio in the total HOAs and coma. This possibly was caused after LASIK by a shape change in the anterior corneal surface because of laser ablation.

Although no detailed information was available for the LASIK procedures in keratectasia eyes, these should have laser ablation aligned to the primary line of sight. If keratectasia was induced mainly by stromal instability due to laser ablation, a symmetrical protrusion of the anterior and posterior corneal surfaces can be expected. However, the distribution pattern of the Zernike terms in keratectasia indicated coma dominance (Figs. 2, 3), and the axis of coma had a specific distribution (Fig. 5). The characteristics of the corneal HOAs in keratectasia were similar to those in keratoconus for both corneal surfaces.[12,13,22]

These results confirmed that the basic strategy for the treatment of keratectasia should be similar to that for keratoconus. To maintain a good quality of vision with spectacles or contact lenses, it will be important to inhibit the progression of keratectasia when the corneal HOAs are still within the acceptable range. For moderate to advanced

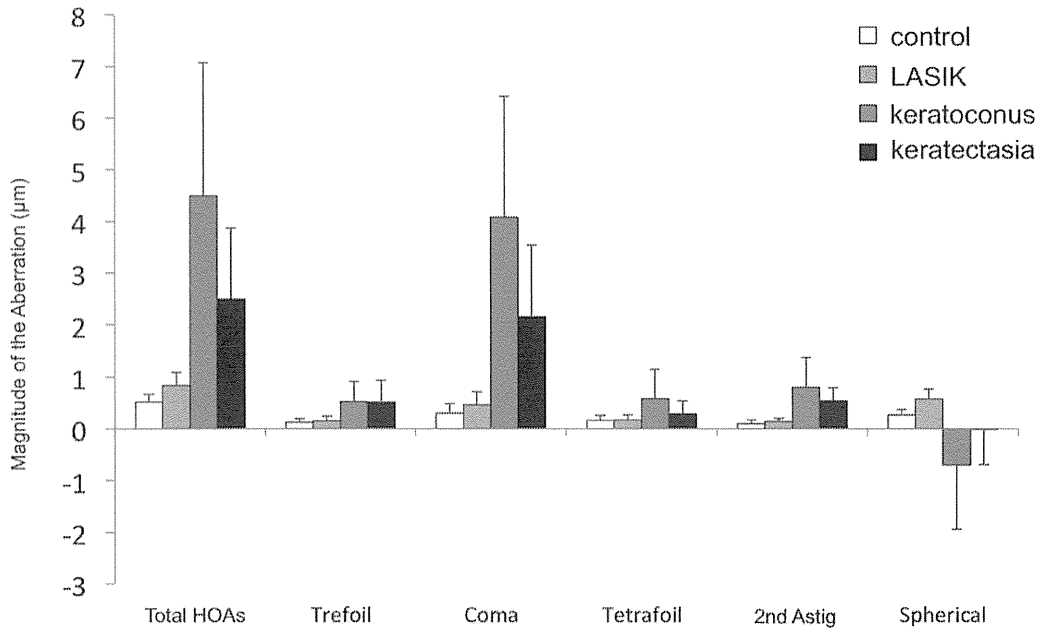

FIGURE 2. The means and standard deviations of the total HOAs and each Zernike term of the anterior corneal surface for the 6-mm diameter. The graph shows the simple averages and standard deviations of the magnitudes of the total HOAs (RMS) and each Zernike term. Keratectasia and keratoconus showed similar coma-dominant patterns in the Zernike terms for the anterior corneal surface. 2nd Astig, secondary astigmatism; spherical, spherical aberration.

keratectasia with the increase in HOAs at the posterior corneal surface, CDVA with RGP contact lens will be limited by the residual HOAs because of the posterior surface.[13,22]

Radleman et al.[23] reported that preoperative topographic abnormality, low residual stromal bed thickness, young age, thin corneas, and high myopia were factors that increased the risk for developing post-LASIK corneal ectasia. Among them, the most significant factor was abnormal topography.

The preoperative abnormal topographic findings seen in keratectasia may have a very early sign of keratoconus. The

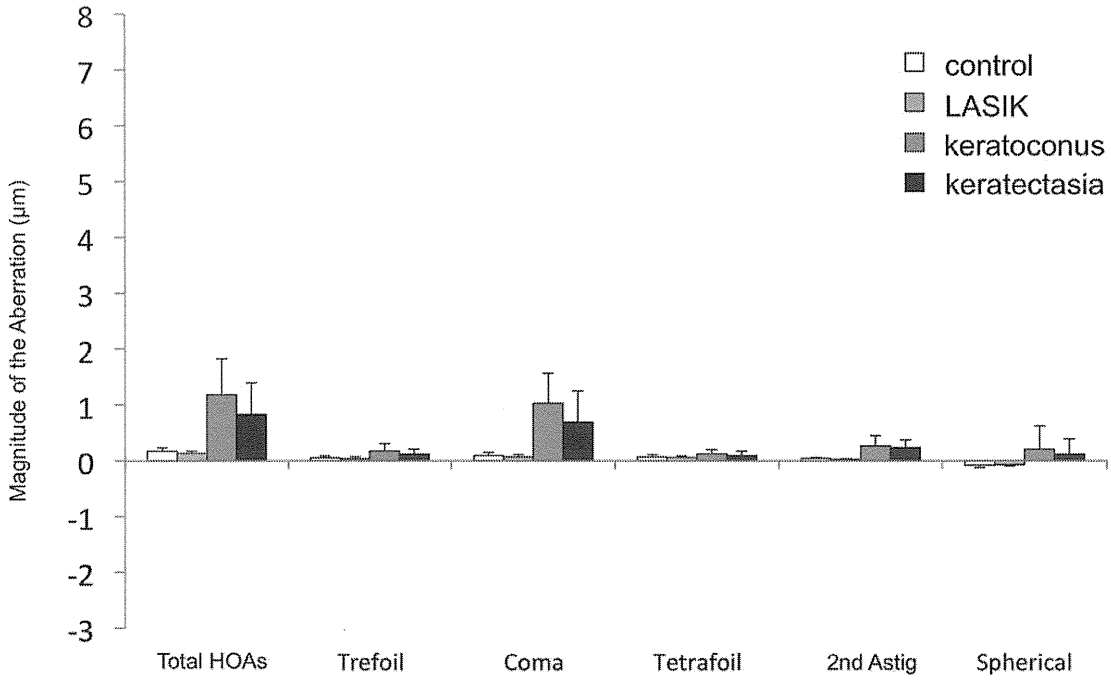

FIGURE 3. The averages and standard deviations of the total HOAs and each Zernike term of the posterior corneal surface for the 6-mm diameter. The graph shows the simple averages and standard deviations of the magnitudes of the total HOAs (RMS) and each Zernike term. Keratectasia and keratoconus showed similar coma-dominant patterns in the Zernike terms also for the posterior corneal surface.

TABLE 2. Statistical Significance (*P* Values) of HOAs by the Steel–Dwass Test

	Total HOAs	Trefoil	Coma	Tetrafoil	Second Astig	Spherical
Anterior surface						
Control vs. LASIK	<0.001*	0.5433	0.0337*	0.9180	0.0613	<0.001*
Control vs. KC	<0.001*	<0.001*	<0.001*	<0.001*	<0.001*	<0.001*
Control vs. ectasia	<0.001*	<0.001*	<0.001*	0.2249	<0.001*	0.9987
LASIK vs. KC	<0.001*	<0.001*	<0.001*	<0.001*	<0.001*	<0.001*
LASIK vs. ectasia	0.0002*	0.0003*	<0.001*	0.4781	<0.001*	0.0206*
KC vs. ectasia	0.0310*	1.0000	0.0492*	0.0924	0.7235	0.3319
Posterior surface						
Control vs. LASIK	0.0113*	0.2442	0.3274	0.8586	0.0001*	0.5104
Control vs. KC	<0.001*	<0.001*	<0.001*	0.0007*	<0.001*	0.0002*
Control vs. ectasia	<0.001*	0.0423*	<0.001*	0.6982	0.0001*	0.0286*
LASIK vs. KC	<0.001*	<0.001*	<0.001*	<0.001*	<0.001*	0.0003*
LASIK vs. ectasia	<0.001*	0.0059*	<0.001*	0.2686	<0.001*	0.0264*
KC vs. ectasia	0.4608	0.6724	0.4955	0.3172	0.9997	0.8993
A/P ratio						
Control vs. LASIK	<0.001*	0.1204	0.0024*	n. s.	<0.001*	n/a
Control vs. KC	0.0262*	0.9958	0.4193	n. s.	0.1089	n/a
Control vs. ectasia	0.9855	0.2133	0.9236	n. s.	0.9236	n/a
LASIK vs. KC	<0.001*	0.1204	0.0184*	n. s.	0.0018*	n/a
LASIK vs. ectasia	0.0012*	0.9913	0.0657	n. s.	0.0206*	n/a
KC vs. ectasia	0.4438	0.2249	0.7719	n. s.	0.8574	n/a

* Statistically significant.

present study also indicated that in keratectasia, the cornea had optical properties similar to those in keratoconus. It will be very important for the prevention of keratectasia after LASIK to discern these specific abnormal findings of the corneal shape in those cases who might be quantitatively predisposed to keratoconus.[24]

The present study had some limitations. Because of the rareness of this disease, the number of keratectasia cases was small. Mild cases of keratectasia were not included, and the changes in HOAs during the course of progression in keratectasia were unknown. The groups of post-LASIK eyes with or without keratectasia included the information of both eyes. The

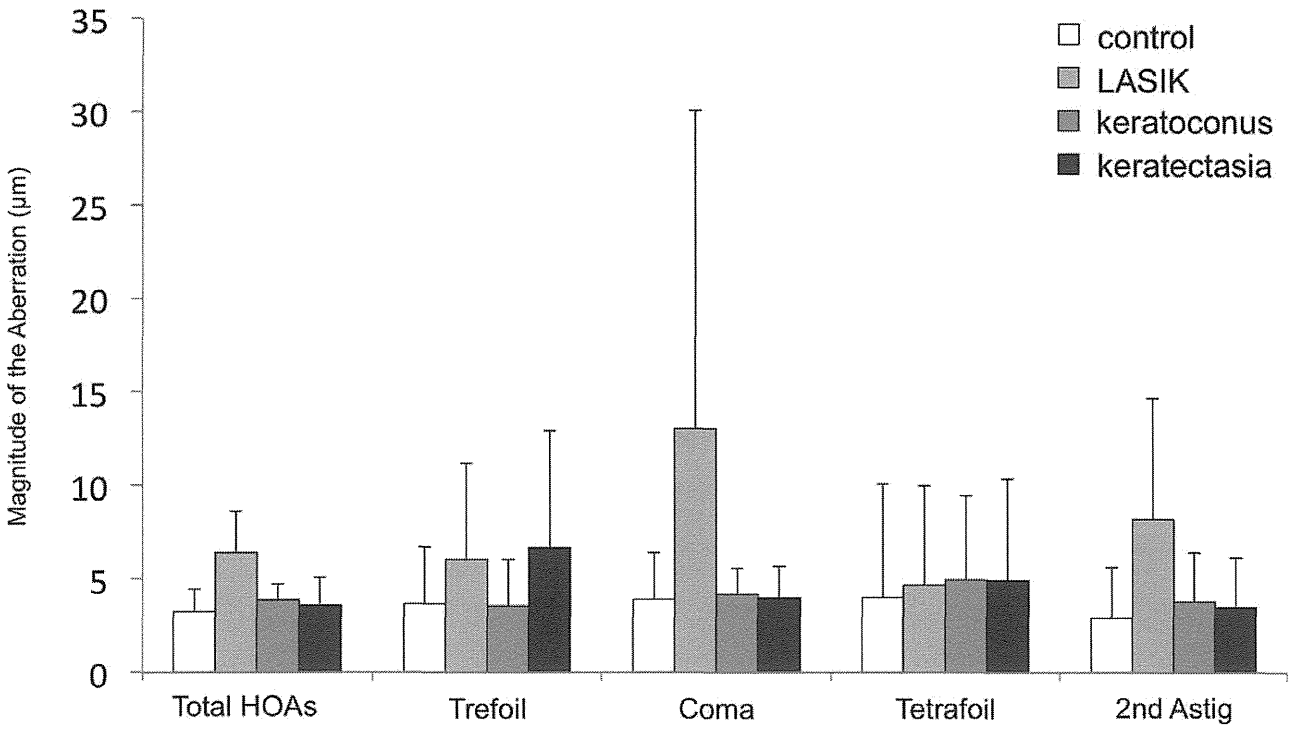

FIGURE 4. The averages and standard deviations of the anterior/posterior ratio of the total HOAs and each Zernike term for the 6-mm diameter. The A/P ratios of total HOAs and coma in LASIK eyes were significantly higher than those in normal eyes.